SYMBIOSIS (2007) 43, 115–127 ©2007 Balaban, Philadelphia/Rehovot ISSN 0334-5114

Observations of variation within the *Amphisorus* genus of symbiotic foraminifera

M.H. Cevasco[1*] and J.J. Lee[2]

[1]Department of Invertebrate Zoology, American Museum of Natural History, Central Park West and 79th Street, New York, NY, 10024, USA, Tel. +1-212-313-7635, Email. megan@amnh.org;
[2]Department of Biology, City College of New York, CUNY, Convent Ave., 138th Street, New York, NY 10031, USA, Email. jjlee@sci.ccny.cuny.edu

(Received July 21, 2006; Accepted October 25, 2007)

Abstract
Initial findings are presented on the morphological variability observed in specimens of larger symbiotic foraminifera within the genus *Amphisorus*. Scanning electron microscope images of seven distinct *Amphisorus* populations collected from Red Sea and Pacific locations are compared to each other and to other genera (*Marginopora* and *Sorites*) within the subfamily Soritinae. Using both test fracture and resin cast images novel features of internal test skeleton are described that expand the morphological breadth of the genus *Amphisorus*. These findings are presented with molecular (18S and 28S) data in a combined phylogenetic analysis which indicates five *Amphisorus* groupings, as well as, the reassignment of *Marginopora kudakajimaensis* to the genus.

Keywords: Soritinae, *Amphisorus*, *Marginopora kudakajimaensis*, SEM

1. Introduction

Among larger reef-dwelling foraminifera (d'Orbigny, 1826) that harbor zooxanthellate endosymbionts, the Sortinae (Ehrenberg, 1839) is a subfamily in which three genera – *Amphisorus* (Ehrenberg, 1839), *Marginopora* (Quoi and Gaimard in Blainville, 1830), and *Sorites* (Ehrenberg, 1839) – are generally recognized. Soritine foraminifera are distinguished by discoid calcareous tests, which are formed by the growth of annular chamber rings (Loeblich and Tappan, 1988). All soritines at early developmental stages have at least a single row of marginal apertures on the test's peripheral face and divide annular chambers into chamberlets with lateral septula (internal calcite partitions) (Gudmundsson, 1994).

Within the Soritinae, the genus *Amphisorus* has been recognized by its internal test architecture, which consists of a duplex skeleton forming chamberlets on either side of an annular canal but lacking a median skeleton (Loeblich and Tappan, 1988; Gudmundsson, 1994). This character combination is distinct from both *Sorites*, which possesses only a single layer of chamberlets, and *Marginopora*, which has a well developed median skeleton (Hofker, 1952; Ross, 1972).

Until recently the genus was monotypic consisting of the type species *Amphisorus hemprichii* (Ehrenberg, 1839). However, the collection of an *Amphisorus* population from the Great Barrier Reef (Australia) that was diagnosably distinct from *A. hemprichii* resulted in the erection of a new species, *Amphisorus saurensis* (Lee et al., 2004), within the genus. Additionally, molecular ribosomal DNA data both support *A. saurensis* as a distinct species within the genus (Lee et al., 2004) and indicate additional variation within Soritinae genera (Holzmann et al., 2001; Richardson, 2001; Garcia-Cuetos et al., 2005). Here we present the morphological and molecular variability found in *Amphisorus* specimens collected from the Red Sea and Pacific locations.

*The author to whom correspondence should be sent.

Presented at the Workshop on Unicellular Symbionts, December 12–13, 2005, Vienna, Austria

2. Materials and Methods

Specimen collection

Soritine specimens were collected by the authors via snorkeling or SCUBA diving (1–24 meters depth) from sea grass beds, clumps of coralline algae, or sandy substrates located adjacent to coral reefs at the following locations: Eilat, Israel (29°32'N, 34°57'E); Oahu, Hawaii (21°24'N, 157°44' W); Kauai, Hawaii (21°52'N, 159°27'W); Lizard Island, Australia (14°39'S, 145°26'E); Puerto Rico (17°58'N, 67°01'W) and Made Island, Antigua (17°06'N, 61°59'W). Specimens were contributed by colleagues from the following locations: Bird Island, Australia (14°41'S, 145°26'E), donated by L. Pearce and L. Vail; Kakaban, East Kalimantan (2°8'N, 118°30'E) and Cebu, Philippines (10°18'N, 124°53'E), donated by W. Renema; Kudaka Island, Japan (26°09'N, 127°53'E), donated by K. Fujita; Ritidian Beach, Guam (13°39'N, 144°51'E), donated by C. Loban; Key Largo, Florida (25°7'N, 80°17'W), Key West, Florida (24°32'N, 80°48'W), and Sand Key, Florida (24°27'N, 80°52'W) donated by P. Hallock; and Zampa Point, Japan (26°19'N, 127°57'E), donated by E. Hirose.

Microscopic preparation

A minimum of 10 specimens from each population of foraminifera obtained were prepared for scanning electron microscope (SEM) examination by first washing each test in distilled water and removing as much surface debris as possible with a red sable brush (#1). The foraminifera then were either scalpel dissected or subjected to a casting technique modified from Hottinger (1979). Both dissected tests and specimen casts were sputter-coated with approximately 10 nm of gold prior to SEM observation. Specimens were observed and imaged in either the Zeiss DSM 940 scanning electron microscope at City College (CUNY) or the Hitachi S-4700 cold-field emission scanning electron microscope at the American Museum of Natural History.

The casting technique required that specimens be prepared for embedding by twice washing each foraminiferal specimen for 30 minutes in propylene oxide. The resin Poly/Bed 812 Embedding Medium then was added to specimens in a 1:2 ratio to the propylene oxide in which they were immersed. The percentage of resin was gradually increased to 100% through three serial medium changes. Specimens were placed in a vacuum chamber after each change to remove air bubbles. Following overnight infiltration of the resin, the specimens were transferred into resin to which the hardener DMP-30 had been added and placed in a 60°C oven for polymerization.

After the specimens were cured, they were ground on a geologist's wheel using 600 grit fine sandpaper and then micro-polished on a felt-wheel. Specimens were ground at transverse angles and in cross-section. The carbonate test exposed through grinding was etched with 1% acetic acid ($C_2H_4O_2$) to create an epoxy cast of the foraminifera to elucidate patterns of connectivity among chamberlets and chambers.

Molecular preparation

Qiagen DNeasy® kits were used to extract DNA from each foraminiferal specimen. The extracted DNA was then subjected to PCR amplification using 2 µl of template in 25 µl reaction tubes of PuReTaq Ready-To-Go™ PCR Beads (GE Healthcare). Although the PCR profile varied depending on the primer set used and the population being amplified, in general the conditions that proved the most successful in amplifying the foraminiferal template required at least 30 cycles of 94° for 30–45 seconds, 49–52° annealing for 30–40 seconds and a 72° extension for 45–60 seconds. Successful amplification products were sequenced in both directions with ABI PRISM BigDye Terminator (Applied Biosystems) and electrophoresed in ABI Prism™ 3730 sequencer (Applied Biosystems). PCR amplification and cycle sequence products were cleaned using the Agencourt® solutions AMPure® and CleanSeq®, respectively.

To develop additional primer sets specific to soritine foraminifera, a cDNA library was generated in which the dinoflagellate endosymbiont cDNA was subtracted from that of the soritine foraminiferal hosts.

Construction of this subtracted cDNA library required that both foraminiferal specimens and dinoflagellates isolated and cultured from foraminiferal hosts were preserved in RNAlater® solution (Ambion™). These specimens were then pulverized on ice with a tissue grinder in a Knotes glass tissue homogenizer. In the foraminiferal specimens, the protoplasm was then separated from the carbonate test remnants by refrigerated centrifugation at 5°C at 6,000 g. The supernatant was then subjected to mRNA extraction following the protocols outlined in the Roche™ mRNA isolation kit. Once ≥2 ng of foraminiferal RNA was obtained, the Clontech SuperSMART™ PCR cDNA Synthesis Kit was used to generate cDNA transcripts. This kit generates cDNA transcripts using an oligo dT primer at the 3' end of the nucleotide string such that the reverse transcriptase enzyme moves from the 3' to the 5' end where the enzymes terminal transferase adds a string of cytosine bases. The kit then attaches an oligo with a guanine (G) sting at the 3' end, thereby allowing for the synthesis of full-length cDNA transcripts.

Subsequent to foraminiferal and dinoflagellate cDNA synthesis, the Clontech PCR-Select™ cDNA Subtraction Kit was used to perform the subtraction of symbiont transcripts from those of host origin. This protocol consisted of an initial restriction enzyme digestion (*Rsa*-I), followed by the ligation of two adaptor oligos to the tester

(foraminiferal cDNA). The tester and driver (symbiont cDNA) then were hybridized and incubated together to allow for the driver transcripts to anneal to each other. A PCR step with nested primers was then performed that amplified only the adaptor-linked tester transcripts that are not of driver origin (i.e. hybridized to the driver cDNA transcripts).

The foraminiferal transcript enriched PCR product was electrophoresed in a low melting point agarose gel such that the transcripts >500 nt were gel extracted. This population of cDNA was then cloned into a bacterial vector using the protocol provided in the TOPO™ TA cloning kit. Cloned transcripts were then amplified and sequenced with the provided M13 primers.

Phylogenetic analyses

Sequences were edited using CodonCode Aligner (CodonCode Corporation) and Geneious© 3.4 (Biomatters Ltd.). When required for analysis, sequence aligments were preformed using the Clustal W software as implemented in Geneious© 3.4 (Biomatters Ltd.) under multiple gap cost regimes. The alignment parameter combination of gap opening cost 15 and gap extension cost 5 produced the most parsimonious solutions in the phylogenetic reconstructions requiring aligned datasets.

The parsimony optimality criterion was implemented in all phylogenetic analyses conducted. Analyses using aligned data (static homology statements) were performed using T.N.T. Version 1.1 (Goloboff et al., 2001). All characters were treated as non-additive and equally weighted with gaps treated as missing data. For each dataset analyzed, 100 replicates of random taxon addition were performed by way of the Wagner tree-building algorithm (Kluge and Farris, 1969). The search strategy implemented used both tree bisection-reconnection (tbr) branch swapping and "new technology" search options of tree drifting and sectorial searches (20 replicates each) to find a globally optimal solution for a given dataset. The tree drifting algorithm implement in TNT aids in finding a globally optimal tree by a process of simulated annealing wherein suboptimal solutions are temporarily accepted with a certain probability (dependant upon both the relative fit and length difference calculations) to help the tree search escape local optima (Goloboff, 1999). Likewise, sectorial searches are heuristic aids for reaching a globally optimal solution wherein selected portions of the tree are subjected to reanalysis and then replaced when a better solution is found (Goloboff, 1999).

Parsimony analyses were also conducted using a dynamic homology approach as implemented in the program POY 4 Beta (Varón et al., 2007). The use of a dynamic homology approach in which homology statements are tree specific (generated during tree building) rather than pre-defined, allowed for the direct optimization of unaligned sequences. The gap cost parameters used in direct optimization were as follows: two for gap opening and one for gap extension. As in the TNT analyses, all characters directly optimized in POY with the optimality criterion of parsimony were treated as non-additive and equally weighted.

Unlike static approaches in which matrix (i.e. alignment) columns are fixed forming statements of primary homology, dynamic programming optimizes characters on a tree as it is being constructed (Wheeler, 1996). The dynamic homology property, while allowing for greater flexibility in tree construction, requires numerous initial Wagner tree builds to provide enough swappable branch arrangements to escape suboptimal solutions. The unaligned datasets analyzed in this study were used to build 200 initial Wagner trees. These trees were then subjected to tbr swapping followed by a round of tree fusing. Tree fusing as it implemented in POY refers to a heuristic algorithm in which clades with identical composition of terminals are exchanged between pairs of trees to escape the local optimum (Goloboff, 1999).

In analyses of the larger datasets with greater than 80 taxa and 2000 total characters (nucleotide and morphology), the parsimony ratchet was implemented to improve the efficiency of searches in finding globally optimal solutions. To augment hill-climbing search strategies (e.g. tbr), the parsimony ratchet escapes local optima by implementing partial changes to a tree based on character conflict without altering the structure of the tree as a whole (Nixon, 1999). In both static and dynamic homology analyses of larger datasets, 50 ratchet iterations were performed subsequent to tbr branch swapping.

Parsimony jackknife support values were calculated for the lowest cost trees generated from both static homology (TNT) and direct optimization (POY) analyses. In the POY analyses, dynamic homology characters were converted to static matrices that could be subjected to jackknife resampling by generating an implied alignment specific to the lowest cost tree. In both programs (TNT and POY) jackknife frequencies were calculated from 1000 pseudoreplicates of matrix resampling without replacement (36% deletion) using random taxon addition and tree bisection-reconnection swapping (Farris, 1999).

3. Results

Morphological character exploration

Below the ordinal level, foraminiferal taxonomy reflects the distribution of designated "key" characters primarily associated with test growth, chamber form, and aperture morphology. Appendix A contains both the matrix of 30 morphological characters constructed from light and electron microscopic observations of soritine populations

and the coding conventions employed in this study. Selected characters from Gudmundsson (1994) and Richardson (2001) that have been incorporated in the current character matrix are indicated in Appendix A. As the soritine groupings corresponding to "key" character distributions vary throughout the literature (e.g. Gudmundsson, 1994; Richardson, 2001) the geographic location of specimens rather than a presumed taxanomic identity is used in the discussion of soritine characters that follows.

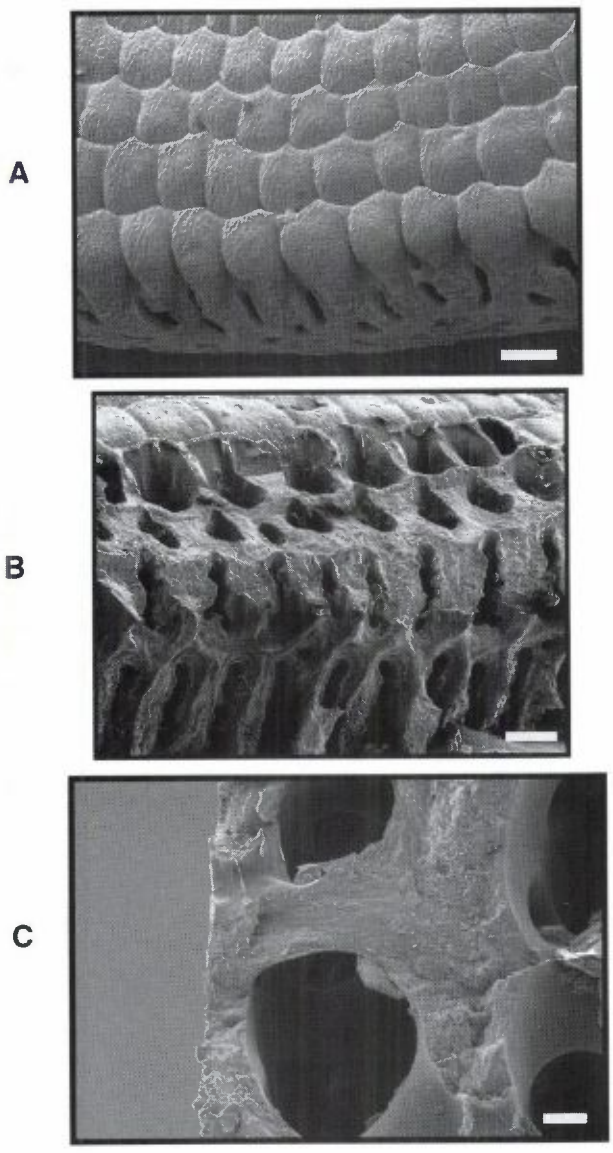

Figure 1. Endoskeletal characters. A) Wavy sutures (character 15) between chamber whorls on Hawaiian (Oahu:1) specimen (scale bar = 25 μm). B) Guam specimen with partial test removed to expose endoskeltal calcite (character 16) dividing chamber whorls into chamberlets (character 17) (scale bar = 35 μm). C) Hawaiian (Poipu) specimen in cross-section showing endoskeletal structure (scale bar = 2 μm).

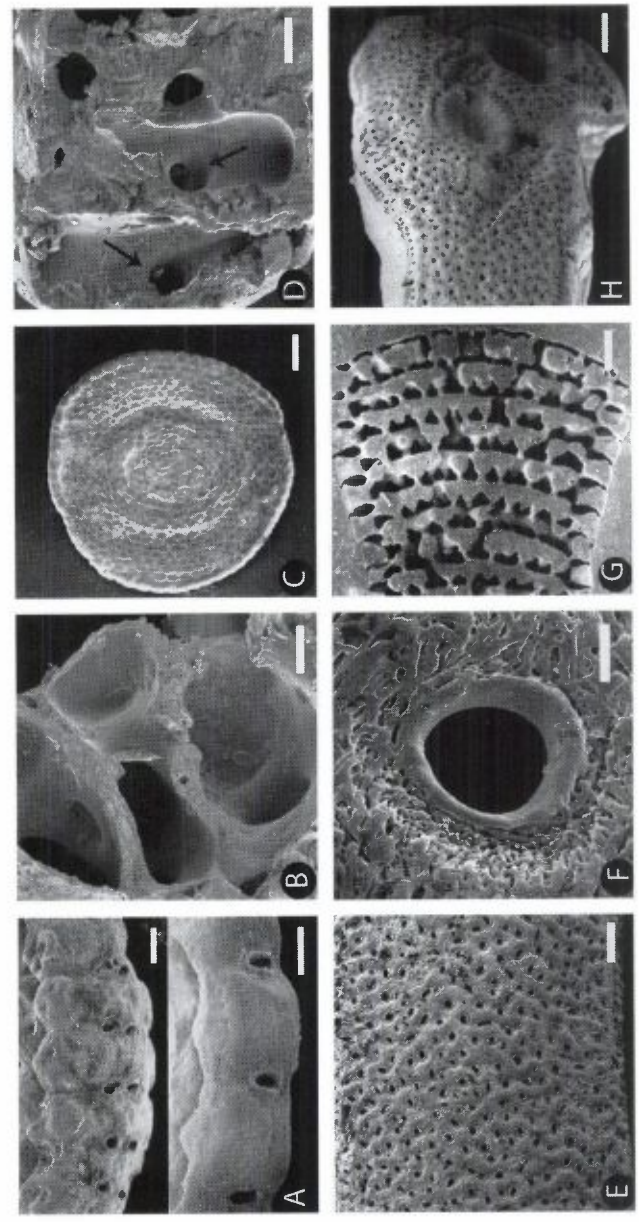

Figure 2. Scanning electron microscope images of morphological characteristics noted in Ritidian Bay:2, Caribbean populations [A–D] and Ritidian Bay:3 Bird Is.:2, Lizard Is., and Oahu:2 populations [E–H]. A) Arrangement of lateral apertures top image = double apertural row, bottom image = single aperture row (scale bars = 20 μm). B) Chamber morphology from above with the top layer of calcite removed (scale bar = 4 μm). C) Whole test showing the general discoid test shape common to all genera within the soritinae (scale bar = 1 mm). D) Cross-section showing chamber morphology and the annular canals (as indicated by the arrows) (scale bar = 15 μm). E) Peripheral (apertural) view showing he shape, number, and placement of marginal apertures (scale bar = 150 μm). F) A single peripheral aperture exhibiting a pronounced lip and generally circular shape (scale bar = 5 μm). G) Resin cast cross-section showing the presence of a well developed median skeleton (black areas) within the chambers (scale bar = 100 μm). H) Peripheral view of an abnormally formed specimen illustrating distinct patterning of marginal vs. median apertures (scale bar = 1.5 mm).

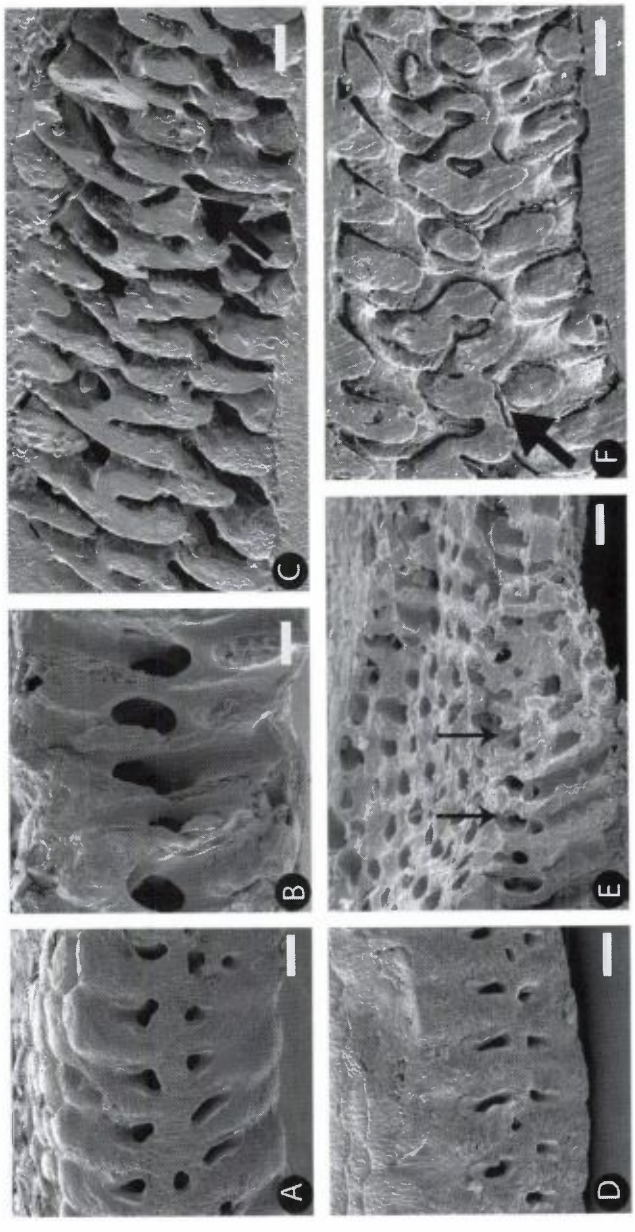

Figure 3. Scanning electron microscope images of soritines from the Red Sea. [A–C] and Guam, Ritidian Bay:1 [D–F] populations: A) Apertural view of an Eilat specimen showing a double row of elongate marginal apertures as well as a median aperture (scale bar = 50 μm). B) Test fracture cross-section of an Eilat specimen showing the annular canals dividing upper and lower offset chamberlets (scale bar = 70 μm). C) Resin cast cross-section showing the cytoplasmic connection between chambers (arrow) (scale bar = 70 μm). D) Apertural view of a Guam specimen showing the double row of elongate marginal apertures and circular median apertures (scale bar = 55 μm). E) Test fracture of a specimen with a portion of chamber tops removed with some annular canals visible (black arrows) (scale bar = 55 μm). F) Resin cast cross-section with the calcite only partially etched to reveal a two-dimensional slice of to illustrate the cytoplasmic connections between chambers (arrow) (scale bar = 70 μm).

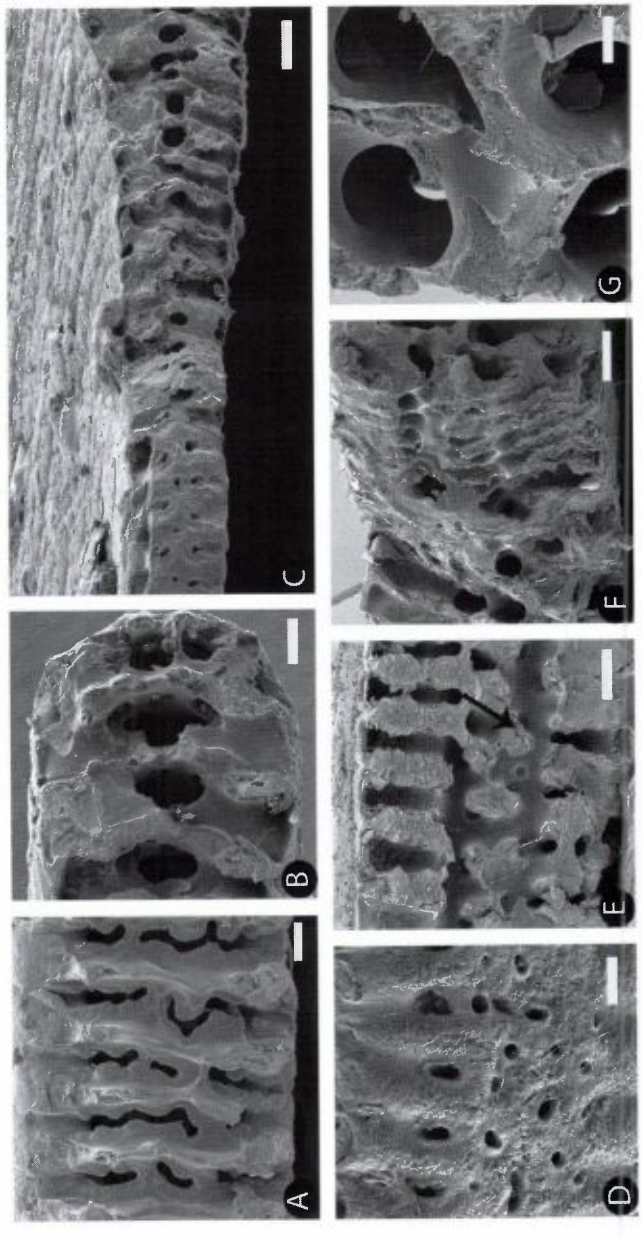

Figure 4. Scanning electron microscope images of specimens from Australia (Bird Island:1) [A–C] and Hawaii (Oahu:1 and Poipu) [D–G]. A) Test fracture with outer chamber removed to expose the aperatural face of the penultimate chamber (scale bar = 25 μm). B) Test fracture cross-section of the outer chambers showing the expansion of the annular canal (scale bar = 55 μm). C) Test fracture cross-section exposing an early chamber apertural face and showing chamber expansion (scale bar = 55 μm). D) Peripheral view of the elongated marginal and irregular medial apertures (scale bar = 25 μm). E) Test fracture of specimen with outer chamber removed showing the presence of simple median calcite structure (arrow) (scale bar = 35 μm). F) Test fracture cross-section specimen showing two annular canals running parallel through chambers (scale bar = 25 μm). G) Test fracture cross-section of the outer chamber whorls showing annular canals and aperture outlets (scale bar = 2 μm).

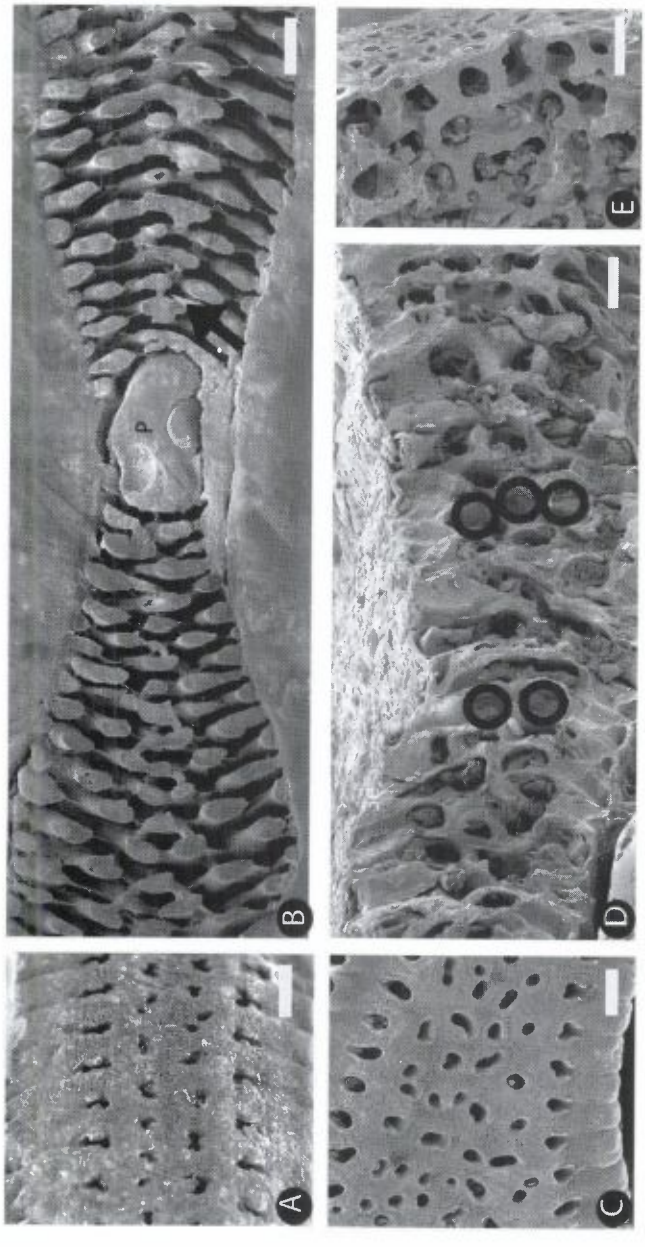

Figure 5. Scanning electron microscope images of specimens from Zampa Point [A–B] and Kudaka Island [C–E] (Japan). A) Peripheral apertures showing two elongate marginal rows and irregular median aperture rows (scale bar = 40 μm). B) Resin cast cross-section of a specimen showing the proloculus (P) and the development of complexity in the median skeleton (black, arrow = example of apertural connection between successive chambers) (scale bar = 35 μm). C) Peripheral apertures of a specimen showing two elongate marginal rows and multiple irregular median apertures (scale bar = 40 μm). D) Test fracture cross-section of a specimen showing the complexity in annular canals (black circles) (scale bar = 100 μm). E) Test fracture cross-section of a specimen showing at the test periphery showing the extent of median skeletal development (scale bar = 60 μm).

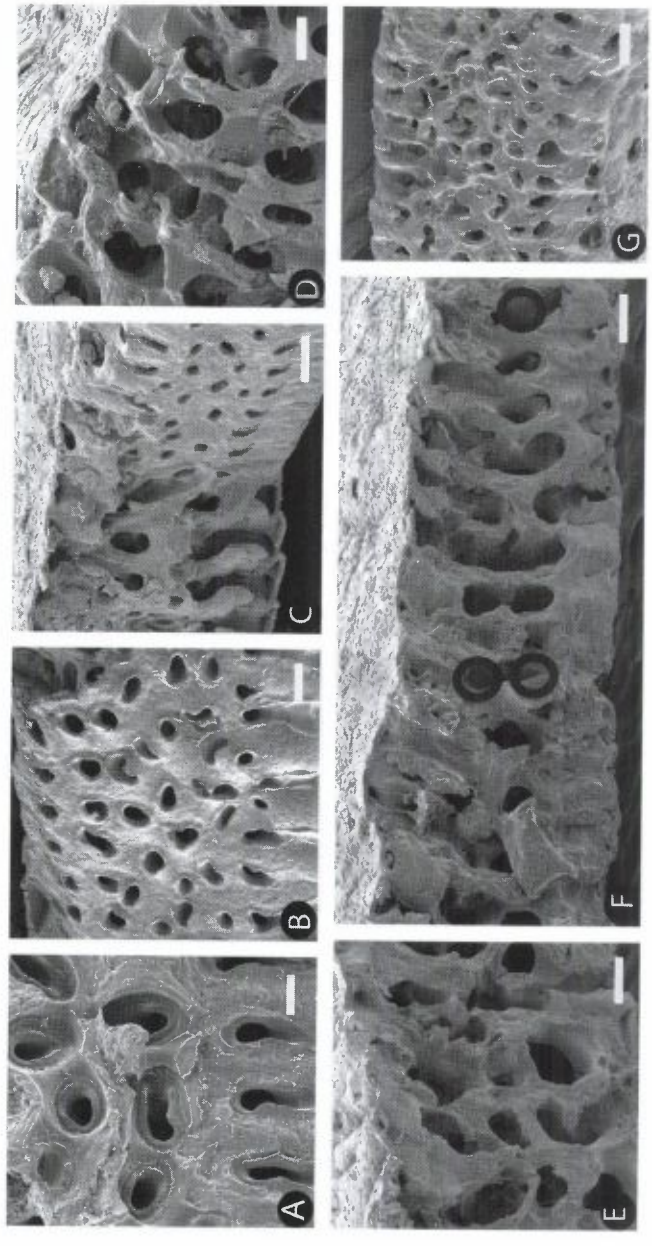

Figure 6. Scanning electron microscope images specimens from East Kalimantan [A–D], and Cebu, Philippines [E–G]. A) Test fracture of a specimen with the outer chamber face removed to apertures in detail (scale bar = 35 μm). B) Peripheral view of a specimen which shows a double row of elongate apertures and multiple irregular median apertures (scale bar = 60 μm). C) Test fracture partial cross-section of a specimen exhibiting a duplex internal skeleton (scale bar = 50 μm). D) Test fracture cross-section of a specimen showing the presence of a double annular canal (scale bar = 60 μm). E) Test fracture cross-section of a specimen exhibiting a series of parallel annular canals (scale bar = 80 μm). F) Test fracture cross-section of a specimen showing the progression from a single to double annular canals (black circles) (scale bar = 80 μm). G) Peripheral view showing a double row of elongate apertures and multiple irregular median apertures (scale bar = 85 μm).

Five matrix characters are present in all sampled soritine populations but absent in the three outgroup taxa included in this study: *Laevipeneroplis proteus* (d'Orbigny, 1839), *Parasorites orbitolitoides* (Hofker, 1930), and *Peneroplis pertusus* (Forskal, 1775). One character observed in living soritine specimens is the presence of dinoflagellate endosymbionts distributed throughout the foraminifer's annular chambers (character 8). Although the outgroup taxa also retain algal symbionts (*Parasorites orbitolitoides* and *Laevipeneroplis proteus* retain chlorophytes; *Peneroplis pertusus* retains rhodophytes), dinoflagellate are only known to form an endosymbiosis in benthic foraminifera within the genera *Amphisorus*, *Marginopora*, and *Sorites*. Another character found in all of the soritine specimens is that of wavy sutures (character 15) between successive chambers corresponding to the chamberlet boundaries (Fig. 1). This character was first proposed by Gudmundsson (1994) and distinguishes soritine morphology from that of other discoid benthic foraminifera. The presence of an endoskeleton (character 16) formed on the inner surface of the chamber wall and consisting of plate-like elements (septula) and/or interseptal pillars was also observed in all observed populations (Figs. 1B and C). The endoskeleton of all the sampled populations creates distinct chamberlets (chamber subdivisions) within each the annular chambers (character 17) (Figs. 1B and C). Finally, connecting each chamberlet to successive chambers is a tubular opening (stolon) in the chamber wall forming an intercameral aperture that allows for a crosswise-oblique flow of protoplasm (character 22) radiating outward from the initial embryonic chambers.

Observations of the endoskeletal morphology of specimens yielded four characters that varied among but not within sampled populations. Septular formation (character 18) was found to exist in three discreet states. Septula spanning across the chamber diameter were found in all of the Caribbean populations and in the Ritidian Bay:2 (Guam) specimens (Figs. 2B and D). Septula that extend from the wall (septum) to the chamber median in an alternating pattern were observed in both the Red Sea and Bird Is.:1(Australia) populations (Fig. 3B). All other Pacific populations – Ritidian Bay:1 and Ritidian Bay:3 (Guam), Kalimantan (Indonesia), Kudaka Is. and Zampa Beach (Japan), Cebu (Philippines), Lizard Is., Pidgeon Point, and Bird Is.:2 (Australia), and all Hawaiian locations – possess septula that span a distance $\leq$ one-fourth of the chamber diameter. A canal connecting the protoplasm of one chamberlet to the next within each annular chamber characterizes all sampled populations. The Caribbean, Red Sea, Ritidian Bay:2 and Bird Is.:1 populations have a single canal running through each annular chamber (Fig. 4B). Six Pacific populations – Kalimantan, Cebu, Kauai and Oahu:1 (Hawaii), Zampa beach and Ritidian Bay:1 –possess a canal that is divided by pillars into two parallel channels (Figs. 5B, 6C, E and F).

Irregular partitioning of the annular canal that creates multiple channels was observed in the remaining sampled Pacific populations: Bird Island:2, Lizard Island, and Pigeon Point, Ritidian Bay:3, Oahu:2, and Japan (Figs. 2G and 5D). In addition to canal partitioning, observations of the growth pattern of the canal area concomitant with test growth (character 20) indicate that the Kalimantan, Cebu, Kudaka Is., Ritidian Bay:3, and all of the Australian populations have canals that expand with test growth (Fig. 3E).

Apertural morphology often provides "key" characters in foraminiferal taxonomy. Seven characters are included in this study relating to the placement, shape, arrangement, and number of apertures observed in the sampled soritine populations. Classically, the presence of marginal apertures has been used to distinguish the genera *Amphisorus* and *Marginopora* from the genus *Sorites* (e.g. Brady, 1881; Loeblich and Tappan, 1987; Gudmundsson, 1994). A double row of marginal apertures (character 23) (Figs. 2H, 3A and D, 5A and C) was observed in all but the Ritidian Bay:2 and Caribbean populations, which possessed lateral apertures (character 25) (Fig. 2A). Lying between the two rows of marginal apertures, medial apertures (character 24) are found in all the populations that possessed marginal apertures, albeit infrequently in the Red Sea specimens (Figs. 2E, 3A and D, 4D, 5A and C, 6B and G).

Aperture shape (character 27) consisted of three primary forms: round to ovate (Fig. 2F), elongate (Fig. 3D), and irregular (Fig. 5C). It was also necessary to code for combinations of the three observed aperture shapes to account for differences in the shape of multiple apertures along a specimen's test periphery. The Ritidian Bay:2, Ritidian Bay:3, Bird Is.:2, Lizard Is., Pigeon Point, Oahu:2, and Caribbean populations have round to ovate apertures (Fig. 2E). The Bird Is.:1 population's apertures are irregular (Fig. 4A). Bird Is.:1 was the only population to possess only irregular apertures. The Ritidian Bay:1, Kauai, Oahu:1, and Red Sea populations were observed to have both round/ovate and elongate shaped apertures (Figs. 4D, 3A and D). The Zampa Beach population was characterized by both elongate and irregularly shaped apertures (Fig. 5A). However, the apertures of the other Japanese population (Kudaka Is.), as well as those from Kalimantan and Cebu show all three primary forms (Figs. 5C, 6B and G).

To normalize the data, the size (i.e., maximum dimension) of apertures was coded relative to chamber height (character 28) rather than by actual dimension. In the Bird Is.:2, Lizard Is., Pigeon Point, Oahu:2, Ritidian Bay:3, Kudaka Is., Kalimantan, Zampa Beach, and Cebu populations, apertures are <1/4 of the height of the final chamber (Figs. 2E and 6C). Apertures ranging in size between 1/4 to 1/2 of chamber height characterize the following populations: Ritidian Bay:1, Red Sea, Bird Is.:1, Kauai, and Oahu:1 (Fig. 3D). The remaining populations of the Ritidian Bay:2 and Caribbean specimens were

observed to have apertures generally greater than 1/2 the height of the chamber's apertural face (Fig. 2A).

Although aperture density (character 29) is necessarily influenced by apertural size, its distribution only partially overlaps that of character 28. With the exception of Zampa Beach, in all other populations where the aperture size was <1/4 chamber height the density of apertures exceeded three per chamberlet (Fig. 5C). The Zampa Beach specimens, however, showed 2–3 apertures per chamberlet, akin to those of the larger apertured Bird Is.:1, Kauai, and Oahu:1 populations. Ritidian Bay:1 and Red Sea specimens possess apertures measuring 1/4–1/2 chamber height and have an apertural density of 1–2 apertures per chamberlet. This apertural density was also found to characterize the Ritidian Bay:2 and Caribbean populations, in which apertural size exceeds 1/2 of the chamber height (Fig. 2D).

Only the Bird Is.:1 and Zampa Beach specimens were found to have apertures in which a calcite rim or lip (character 30) was absent (Fig. 5A).

The patterns of character distribution across the specimens examined approximate those of the soritine genera *Sorites*, *Amphisorus*, and *Marginopora*. Among the Caribbean and Ritidian Bay:2 populations, which correspond to the genus *Sorites*, no consistent morphological differences were noted. This distribution agrees with Gudmundsson (1994) in the lack of a diagnosable difference between *S. orbiculus* and *S. marginalis*. In contrast to the findings of Richardson (2001), pits were not observed in the chamber walls of any of the Caribbean or Ritidian Bay specimens (Fig. 2C) and so could not be used to distinguish *S. marginalis*.

An identical character distribution also occurs among the Lizard Is., Pigeon Point, and Oahu:2 specimens, which correspond to the genus *Marginopora*. Bird Is.:2 and Ritidian Bay:3 specimens exhibit a similar pattern of character states and differ only in that they are slightly larger and in that the Bird Is.:2 population exhibits the autapomorphic trait of loss of its embryonic chambers in the later stages of growth.

The two Red Sea populations – Eilat: stones collected from hard substrates at a depth of 15 m and Eilat: *Halophyla* collected from phytal substrates at a depth of 5 m – show identical character distributions that correspond to the genus *Amphisorus*. Although distinguished from the Eilat populations by annular canals that are divided by interseptal pillars, Hawaiian specimens (Kauai and Oahu:1) also were found to share an "*Amphisorus*-like" character distribution. Similarly the patterns of both the Zampa Beach and Ritidian Bay:1 specimens resemble those of the Hawaiian "*Amphisorus*-like" specimens. The characters observed in the Bird Is.:1 specimens are unique among the populations examined and match those described for the species *Amphisorus sauronensis* (Lee et al., 2004).

The Cebu and Kalimantan populations show identical character distribution patterns, although it was not clear prior to phylogenetic analysis to which genus they most closely align. Similarly, this pattern found in the Kudaka Is. specimens lacks an obvious generic affinity and could explain the ambiguity of the placement of Kudaka soritines first within *Marginopora* by Gudmundsson (1994) and then within *Amphisorus* (Holzmann et al., 2001; Richardson, 2001).

Molecular character exploration

This research aimed to expand the extant molecular data set to resolve the phylogenetic relationships among soritine taxa. Multiple approaches were attempted to find additional molecular markers beyond the ribosomal small subunit (SSU rDNA) used by Holzmann et al. (2001) appropriate to resolving relationships in lower level taxa. Although many of the attempts were unsuccessful, one approach, in which the soritine sequences generated from a subtracted DNA library were found by a BLAST query to be similar to the large subunit sequences of other foraminiferan groups, was used to design ribosomal large subunit (LSU rDNA) primers for the Soritinae.

Table 1. Sequence primers for soritine foraminifera used in this work.

Primer	Sequence 5'→3'	Reference
SSUrDNA		
SA10 (f)	CTCAAAGATTAAGCCATGCAAGTGG	Holzmann et al., 2001
S6R (f)	GGGCAAGTCTGGTGC	Holzmann et al., 2001
S12 (f)	CTACCAAAAGCGAAAGC	Holzmann et al., 2001
S14F3 (f)	ACGCAMGTGTAAACTTG	Holzmann et al., 2001
S13 (r)	GCAACAATGATTGTATAGGC	Holzmann et al., 2001
S17 (r)	CGGTCACGTTCGTTGC	Holzmann et al., 2001
LYS1 (r)	CTCCAACTATCTCCATCGA	Garcia-Cuetos et al., 2005
LSUrDNA		
F5LSU (f)	CTGACGTGCAAATCGTTRCCGCCT	This study
R4LSU (r)	CTTCCATGGCCACCGTCCTGCTGTC	This study

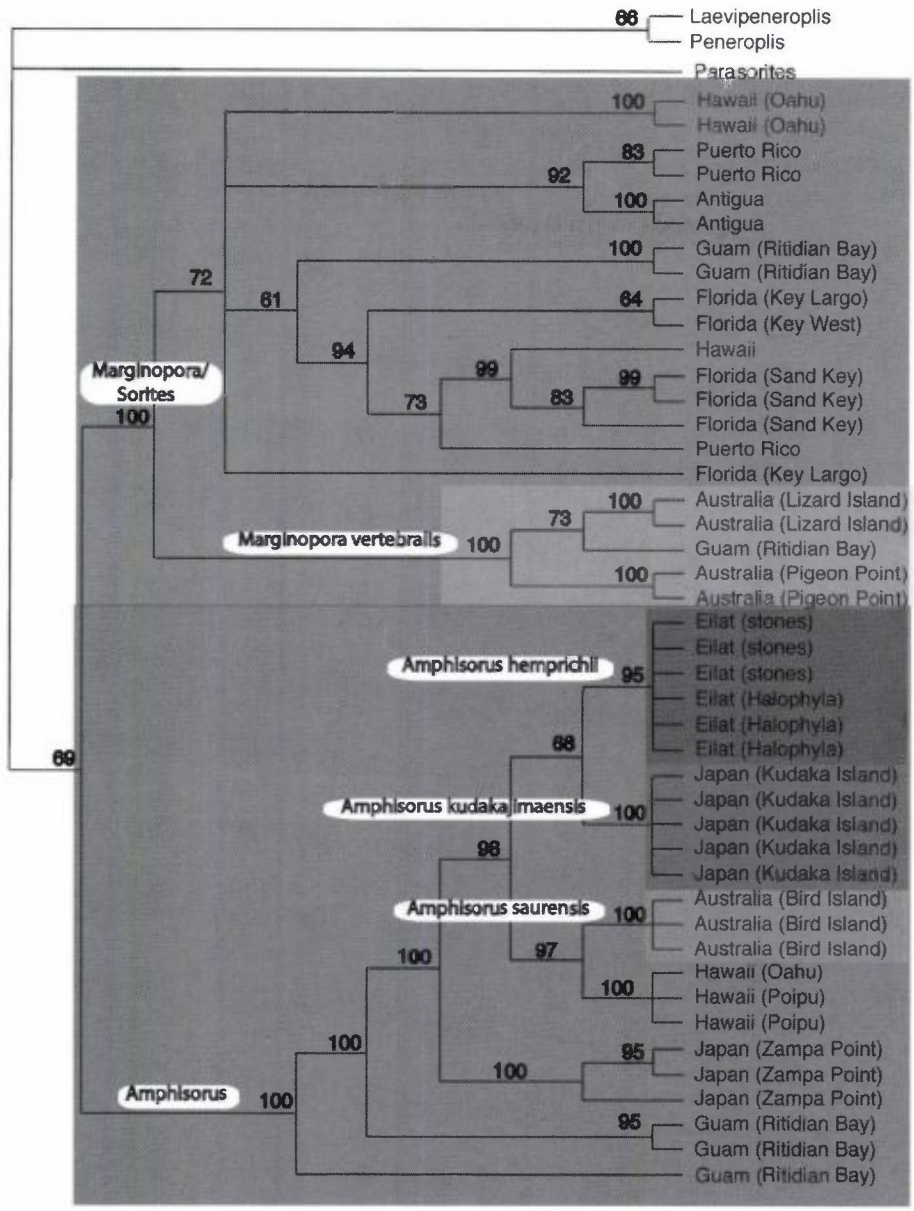

Figure 7. Strict Consensus Parsimony Tree (1917 steps). Generated from five equally parsimonious solutions resulting from TNT analyses of ribosomal DNA (1762 nucleotides) for 47 taxa. Jackknife support values >50 are indicated at the nodes. Grayscale shading denotes major clade divisions: Upper block = *Sorites* and *Marginopora* (*Marginopora vertabralis* clade shaded); Lower block = *Amphisorus* clades (shaded regions = *A. hemprichii*, *A. kudakajimaensis*, *A. saurensis*).

The small 450 nt section of LSU rDNA contains a short variable region (~50 nt) that likely corresponds a to loop structure in the molecule. However, the most notable variability in the sequence is specific to the Zampa Beach specimens. Each of the three Zampa Beach sequences contains multiple unique sections of 4–100 nt found between conserved regions shared with the other taxa. The structural affinity of these sections has not been determined.

In addition to the LSU sequences, SSU rDNA sequences were recovered using the primers of Holzmann et al. (2001) and Garcia-Cuetos et al. (2005). Table 1 contains a list of the primers used in this study.

When concatenated, these primer sets cover the majority of the small subunit genes. Successful amplification using these primers varied depending on population and specimen preservation. Often, slight adjustments in the PCR profile implemented (e.g., changing the annealing temperature) improved results for one set of samples, while worsening the yield in another set. Amplifying shorter fragments within longer read primer sets was another fairly successful tactic to improve yields. For example, fragments of about 700 nt in length that were unable to be amplified in some populations using the primer pair S12 (forward) and S17 (reverse) often would amplify a shorter fragment of 400 nt

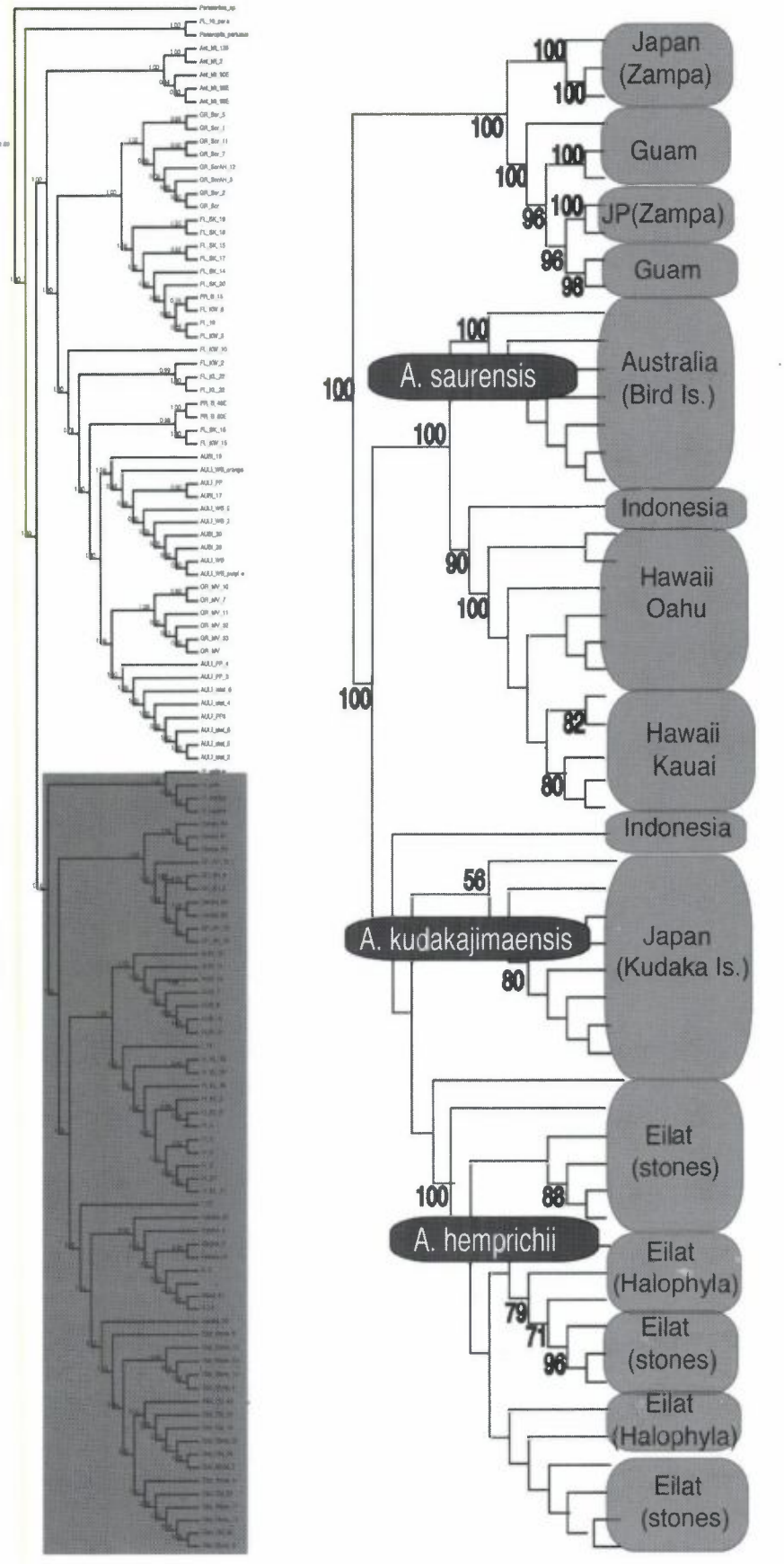

Figure 8. Parsimony Tree (4431 steps). Generated from dynamic homology characters using POY. Partial large and small subunit ribosomal DNA as well as morphological data were included in this analysis (2687 characters) for 114 taxa. Jackknife support values >50 are indicated at the nodes. The clades within the genus *Amphisorus* are enlarged with the named species.

using the primer pair S14F3 and S17. This approach maximized the number of taxa for which sequence data was collected but also created pockets of missing data.

To avoid discarding data, three molecular data sets were constructed: a complete 48 taxa data set of partial SSU and LSU sequences (1762 nt), and an 112 taxa data set of partial SSU and LSU sequences (2717 nt) and morphology which is approximately 80% complete.

Phylogenetic results

The static homology parsimony analysis of 47 taxa with complete sequence coverage of 1762 nt spanning portions of both the small and the large ribosomal subunits yielded five equally parsimonious solutions (trees) 1917 in length. The strict consensus of the static homology trees provided in Fig. 7 shows two major groupings of soritine foraminifera with high support (jac=89). The first major soritine clade is divided further into separate *Marginopora* and *Sorites* specimen clades. The other clade contains all of the *Amphisorus* specimens from the Red Sea and Pacific Ocean basins. Within the *Amphisorus* clade, Hawaiian specimens form a sister group to the Australian (Bird Island) specimens with high support (jac=100). Strong support (jac=100) was also recovered for the sister relationship between *Amphisorus* specimens from Kudaka Island, Japan and Eilat, Israel. This analysis also places the South East Asian *Amphisorus* populations in separate clades often not sister to each other (e.g. Kudaka-Island's non-sister relationship with a population of geographically close Japanese *Amphisorus* specimens from Zampa point.

The combined analysis using direct optimization of ssu and lsu rDNA sequences with the morphological data set yielded a single tree of 4431 steps (Fig. 8). The static homology parsimony analysis in TNT recovered three minimum length trees of 4477 steps. As in the static homology analysis, two major clades (jac=100) were recovered. One major clade contained the *Marginopora* and *Sorites* genera (not shown) and the other clade consisted of specimens within the genus *Amphisorus* (Fig. 8). *Amphisorus* clade is divided into five major groups consisting of the following populations: 1) Okinawa (JP) and Guam, 2) Australia, 3) Hawaii, 4) Kudaka- Island (JP), and 5) Eilat (IS). The two Indonesian specimens included in the analysis placed separately within the *Amphisorus* group, one placed inside the Australian/Hawaiian clade as sister to the Hawaiian specimens and the other as sister to the *Amphisorus* specimens collected in Kudaka Island, Japan.

The phylogenetic analyses conducted in this work reveal biogeographic partitioning at both the generic and population levels in terms of morphological types. Despite the polyphyly of *Sorites* and *Marginopora* populations, only the *Sorites* morphological type was recovered from Atlantic populations. All morphological variants (spanning all genera), however, were recovered from Pacific sampling locations.

At the population level the analyses revealed discreet morphologies within the genus *Amphisorus* in Indo-Pacific populations. Distinct *Amphisorus* morphologies were recovered which correspond to five clades (Guam/Okinawa, Kudaka Island, Australia, Hawaii, and Red Sea). Interestingly, this pattern distinguishes the Okinawa (Zampa Point) population as separate from the neighboring Kudaka Island population.

4. Discussion

This work presents the first analyses of soritine foraminifera to include both nucleotide and morphological characters. Previously, the most comprehensive analysis of this foraminiferal subfamily to include over 1000 base pairs was that presented in Garcia-Cuetos et al. (2005). The inclusion of large subunit rDNA variable region sequences and morphological characters to the analyses improved phylogenetic resolution and to contribute to a better understanding of the diversity contained within the soritine genus *Amphisorus*.

Previously unrecognized patterns of diversity were revealed within *Amphisorus* genus. Three species that correspond to distinctive phenotypes are currently recognized within the genus: *Amphisorus hemprichii* with an annular canal having a constant diameter throughout chamber whorls, (*Amphisorus*) *kudakajimaensis* with an irregularly partitioned annular canal that is expanded in outer whorls, and *Amphisorus saurensis* with a large diameter (>15 mm) and large irregularly shaped medial apertures. Each of these taxa is recovered molecularly as a separate clade. Moreover, even specimens collected from different substrates (phytal vs. stone) and depths (1 m vs.16 m) in the Red Sea still grouped as a single *Amphisorus hemprichii* clade.

In addition to the named species, a well-supported clade was recovered that contained the Hawaiian (Oahu and Kauai) morphologically indistinguishable *Amphisorus* specimens. Although the Hawaiian specimens are morphologically similar to the *A. hemprichii* except in that Hawaiian populations possess a double row of annular canals rather than a single canal and exhibit truncated septular heights less than a quarter of the total chamber height, molecularly they consistently form a sister clade to *A. saurensis*. Distinct morphological differences between *A. saurensis* and the Hawaiian populations including the double row of annular canals and exhibiting elongate rather than irregularly shaped apertures, however, indicate these populations may constitute a distinct Hawaiian species.

The populations collected off of Zampa Point, Okinawa, Japan and from Ritidian Bay, Guam, were also found to form a well-supported clade, notwithstanding their morphological differences (e.g. the presence lipped

apertures and lower apertural density in the Guam population). It is notable that the support for this Guam and Okinawan clade was high (jac=100) despite large (20–50 nt) insertions in the lsu rDNA of the Okinawan specimens. The conflation of the Okinawan population with the Guam population rather than its nearest geographic neighbor (Kudaka Island population) was unexpected and merits further fine-scale biogeographic investigation. The variable placement of the two Indonesian *Amphisorus* specimens is likely a product of missing data as only partial sequences were recovered from them due to poor specimen preservation.

In contrast to the assumption often made that South East Asian soritine populations with "*Amphisorus*-like" morphologies are *A. kudkajimaensis* (e.g. Holzmann et al., 2001), the analyses conducted in this study indicate that *A. kudakajimaensis* is distinct both morphologically and molecularly from other Pacific *Amphisorus* populations, even those collected from nearby sites (i.e. Zampa beach, Okinawa, Japan). Moreover, these analyses indicate that *A. hemprichii* may have a range limited to the Red Sea and may not be the globally distributed species encompassing all other observed *Amphisorus*-like morphologies as was previously believed (see Loeblich and Tappan, 1987). The previously unrecognized diversity in the genus *Amphisorus* both molecularly and morphologically that was revealed in these analyses indicates the need for possible taxonomic revision of this genus.

Acknowledgements

This work was supported in part by the Learner-Gray Fund for Marine Research and by the Horace W. Stunkard Fund for Symbiosis Research. Part of this research will be included in the dissertation work of M. Cevasco. The authors would like to thank all of their colleagues who contributed specimens for this work. We also would like thank Dr. Mark Siddall for supporting the molecular component of this study and Jacob L. Mey for facilitating our access to the Microscopy and Imaging Facility, American Museum of Natural History.

REFERENCES

Altschul, S.F., Gish, W., Miller, W., Myers, E.W., and Lipman, D. 1990. Basic local alignment search tool. *Journal of Molecular Biology* **215**: 403–410.

d'Orbigny, A. 1826. Tableau Methodique de la Classe des Cephalopodes. *Annales des Sciences Naturelles Paris* (Serie 1) **7**: 245–314.

Ehrenberg, C. 1839. Ueber die Bildung der Kreidefelsen und des Kreidemergels durch unsichtbare Organismen. *Physikalische Abhandlungen der Königlichen Akademie der Wissenschaften zu Berlin.* 1838 Berlin, Jahrgang (1839): 59–147.

Farris, J.S. 1999. XAC program and documentation. Swedish Natural History Museum. Stockholm, Sweden.

Garcia-Cuetos, L. Pochon, X., and Pawlowski, J. 2005. Molecular evidence for host-symbiont specificity in soritid foraminifera. *Protist* **156**: 399–412.

Goloboff, P. 1999. Analyzing large data sets in reasonable times: solutions for composite optima. *Cladistics* **15**: 415–428.

Goloboff, P., Farris, J.S., and Nixon, K. 2001. TNT (Tree analysis using New Technology) Version1.1. Published by the authors, Tucamán, Argentina.

Gudmundsson, G. 1994. Phylogeny, ontgeny and systematics of recent Soritacea Ehrenberg 1839 (Foraminiferida). *Micropaleontology* **40**: 101–155.

Hofker, J. 1952. Recent Peneroplidae, Pt.4. *Journal of Microscopical Society, London* **73**: 40–46.

Holzmann, M., Hohenegger, J., Hallock, P., Piller, W.E., and Pawlowski, J. 2001. Molecular phylogeny of large miliolid foraminifera (Soritacea, Ehrenberg, 1839). *Marine Micropaleontology* **43**: 57–74.

Hottinger, L. 1979. Araldit als Helfer der Mikropaläontologie. *Ciba-Geigy Aspekte* **3**: 1–10.

Kluge, A.G. and Farris, J.S. 1969. Quantitative phyletics and the evolution of anurans. *Systematic Zoology* **18**: 1–32.

Lee, J.J., Burnham, B., and Cevasco, M. 2004. A new modern soritid foraminifer from the Lizard Island Group (Great Barrier Reef, Australia). *Micropaleontolgy* **50**: 357–368.

Loeblich, A. and Tappan, H. 1988. *Foraminiferal Genera and Their Classification.* Van Nostrand Reinhold, New York, 970 pp.

Quoi, J.R. and Gaimard, P. 1830 Mollsques, vers et Zoophytes. *Dictionnaire des Sciences Naturelles.* Blainville, H., ed. Levrault, F. Paris.

Richardson, S. 2001. Endosymbiont change as a key innovation in the adaptive radiation of Soritida (foraminifera). *Paleobiology* **27**: 262–289.

Ross, C.A. 1972. Biology and ecology of *Marginopora vertebralis* (Foramininferida), Great Barrier Reef. *Journal of Protozoology* **19**: 181–192.

Varón, A., Vinh, L.S., Bomash, I., and Wheeler, W. 2007. POY 4 Beta. American Museum of Natural History at http://research.amnh.org/scicomp/projects/poy.php.

Wheeler, W.C. 1996. Optimization alignment: the end of multiple sequence alignment in phylogenetics? *Cladistics* **12**: 1–9.

Appendix A: Character list

1) *Biconvex Test: 0 = absent; 1 = present
2) Biconcave Test: 0 = absent; 1 = <5° from proloculus to margin; 2 = ≥5° proloculus to margin
3) *Biumbilicate Test: 0 = absent; 1 = present
4) *Keel: 0 = absent; 1 = present
5) Avg. Test Diameter: 0 = ≤5mm; 1 = >5≤15 mm; 2 = >15 mm
6) Creased Test Margin: 0 = absent; 1 = present
7) Common loss of Embryonic Chambers in Microspheric Test: 0 = absent; 1 = present
8) Dinoflagellate Symbionts: 0 = absent; 1 = present
9) *Planispiral Growth Stage: 0 = absent; 1 = present
10) *Annular Growth Stage: 0 = absent; 1 = present
11) *Flabelliform Chambers: 0 = absent; 1 = present
12) Vorhof: 0 = absent; 1 = <1/2 whorl; 2 = >1/2 whorl
13) *Advolute Coiling in Microspheric Test: 0 = absent; 1 = present
14) *Involute Coiling in Microspheric Test: 0 = absent; 1 = present
15) **Sutures between Chambers: 0 = straight; 1 = wavy
16) Endoskeleton: 0 = absent; 1 = present
17) Chamberlets: 0 = absent; 1 = present
18) Septula: 0 = absent; 1 = spanning chamber diameter; 2 = extending to chamber median; 3 = extending ≤1/4 chamber diameter
19) Annular Canal(s): 0 = absent; 1 = single; 2 = divided into 2 parallel channels; 3 = irregularly partitioned
20) Annular Canal(s) Area: 0 = absent; 1= constant; 2 = expanded in outer whorls
21) *Pillars: 0 = absent; 1 = present
22) Crosswise-oblique Stolon System: 0 = absent; 1 = present
23) **Double Row of Marginal Apertures: 0 = absent; 1 = present
24) **Medial Apertures: 0 = absent; 1 = present
25) *Lateral Row of Apertures: 0 = absent; 1 = present
26) *Longitudinal Aperture Furrow: 0 = absent; 1 = present
27) Aperture Shape: 0 = round/ovate; 1 = elongate; 2 = irregular; 3 = round & elongate; 4 = round & irregular; 5 = elongate & irregular; 6 = round, elongate & irregular
28) Relative Aperture Size: 0 = <1/4 chamber height; 1 = 1/4–1/2 chamber height; 2 = >1/2 chamber height
29) Aperture Density: 0 = N/A; 1=1–2 per chamberlet; 2 = 2–3 per chamberlet; 3 = 4+ per chamberlet
30) Aperture lips: 0 = absent; 1 = present

*Character from Richardson (2001); **Character from Gudmundsson (1994).

Distribution of characters

Sampled populations																														
Laevipeneroplis proteus	1	0	0	1	0	0	0	0	1	0	1	0	1	1	0	0	0	0	0	0	0	0	0	0	0	1	0	0	0	1
Parasorites orbitolitoides	0	0	0	1	0	0	0	0	1	1	1	0	0	0	0	1	1	0	0	0	0	0	0	0	0	1	0	2	0	1
Peneroplis pertusus	0	0	1	1	0	0	0	0	1	0	1	0	0	1	0	0	0	0	0	0	0	0	0	0	0	0	0	0	0	1
Antigua (Made Island.)	0	0	0	0	0	0	0	1	1	1	1	0	1	0	1	1	1	1	1	1	0	1	0	0	1	0	0	2	1	1
Australia (Bird Island:1)	0	1	0	0	2	0	0	1	1	1	1	1	1	0	1	1	1	2	1	2	0	1	1	1	0	0	2	1	2	0
Australia (Bird Island:2)	0	2	0	0	2	0	1	1	0	1	0	2	1	0	1	1	1	3	3	2	1	1	1	1	0	0	0	0	3	1
Australia (Lizard Island)	0	2	0	0	1	1	0	1	0	1	0	2	1	0	1	1	1	3	3	2	1	1	1	1	0	0	0	0	3	1
Australia (Pigeon Point)	0	2	0	0	1	1	0	1	0	1	0	2	1	0	1	1	1	3	3	2	1	1	1	1	0	0	0	0	3	1
Florida (Sand Key)	0	0	0	0	0	0	0	1	1	1	1	0	1	0	1	1	1	1	1	1	0	1	0	0	1	0	0	2	1	1
Florida (Key West)	0	0	0	0	0	0	0	1	1	1	1	0	1	0	1	1	1	1	1	1	0	1	0	0	1	0	0	2	1	1
Florida (Key Largo)	0	0	0	0	0	0	0	1	1	1	1	0	1	0	1	1	1	1	1	1	0	1	0	0	1	0	0	2	1	1
Guam (Ritidian Bay:1)	0	2	0	0	1	0	0	1	1	1	1	1	1	0	1	1	1	3	2	1	1	1	1	1	0	0	3	1	1	1
Guam (Ritidian Bay:2)	0	0	0	0	0	0	0	1	1	1	1	0	1	0	1	1	1	1	1	1	0	1	0	0	1	0	0	2	1	1
Guam (Ritidian Bay:3)	0	2	0	0	2	0	0	1	0	1	0	2	1	0	1	1	1	3	3	2	1	1	1	1	0	0	0	0	3	1
Hawaii (Kailua, Oahu:1)	0	1	0	0	1	0	0	1	1	1	1	1	1	0	1	1	1	3	2	1	1	1	1	1	0	0	3	1	2	1
Hawaii (Kailua, Oahu:2)	0	2	0	0	1	0	0	1	0	1	0	2	1	0	1	1	1	3	3	2	1	1	1	1	0	0	0	0	3	1
Hawaii (Poipu, Kauai)	0	1	0	0	1	0	0	1	1	1	1	1	1	0	1	1	1	3	2	1	1	1	1	1	0	0	3	1	2	1
Indonesia (E. Kalimantan)	0	1	0	0	2	0	0	?	1	1	1	1	1	0	1	1	1	3	2	2	1	1	1	1	0	0	5	0	3	1
Japan (Kudaka Island)	0	2	0	0	2	0	0	1	1	1	1	2	1	0	1	1	1	3	3	2	1	1	1	1	0	0	5	0	3	1
Japan (Zampa Beach, OK)	0	2	0	0	2	0	0	1	1	1	1	1	1	0	1	1	1	3	2	1	1	1	1	1	0	0	4	0	2	0
Philippines (Cebu)	0	1	0	0	2	0	0	?	1	1	1	1	1	0	1	1	1	3	2	2	1	1	1	1	0	0	5	0	3	1
Puerto Rico (La Parguera)	0	0	0	0	0	0	0	1	1	1	1	0	1	0	1	1	1	1	1	1	0	1	0	0	1	0	0	2	1	1
Red Sea (Eilat: *Halophyla*)	0	1	0	0	1	0	0	1	1	1	1	1	1	0	1	1	1	2	1	1	0	1	1	1	0	0	3	1	2	1
Red Sea (Eilat: stones)	0	1	0	0	1	0	0	1	1	1	1	1	1	0	1	1	1	2	1	1	0	1	1	1	0	0	3	1	2	1